

Multicopter Configuration Trades Informed by Handling Qualities for Urban Air Mobility Application

Shannah Withrow-Maser
Aerospace Engineer
Ames Research Center
Moffett Field, CA, USA

Carlos Malpica
Aerospace Engineer
Ames Research Center
Moffett Field, CA, USA

Keiko Nagami
Engineering Student Trainee
Ames Research Center
Moffett Field, CA, USA

ABSTRACT

Many contemporary Advanced Air Mobility (AAM), and more specifically, urban air mobility (UAM) vehicle designers are attracted to variable rotor speed-controlled designs with multiple rotors because of the great potential for mass savings compared to more traditional, variable blade pitch-controlled vehicles. These designs are based on the assumption that the stability and control of recreation or basic utility-sized drones can be scaled to larger passenger-sized vehicles. Previous work had shown the challenges in stabilizing passenger-sized quadcopters. In this study, power constraints were made less restrictive and varied, allowing more control power. Motor parameters such as efficiency, nominal voltage and current operating point, and rise time of the rotor speed controller step response were studied. By fixing the efficiency of the motor to 95% and assuming a motor voltage to current ratio of 2.0 (previously, assumed to be 1.0), the authors were able to stabilize the quadcopter in the roll axis because this allowed the vehicle to achieve adequate rise times between 0.4 and 0.8 s. This motor optimization was extended to a hexacopter and octocopter designed to the same payload size and mission as the quadcopter. The three vehicle configurations and their motor speed controllers were compared. It was found that while hexacopter and octocopter required more mass and overall power; all three configurations had similar margins required for control. However, the hexacopter and octocopter were able to use this power margin to achieve lower rise times (i.e. the vehicle responded more quickly to pilot inputs) than the quadcopter, with the octocopter having the lowest rotor response rise time of the three vehicle configurations studied.

NOTATION

A	Bare-airframe stability derivative matrix	K_e	Motor back-EMF constant (Vs)
A_{rms}	Actuator (motor current) usage metric	K_i	Integral ESC feedback gain
B	Motor friction and viscous losses coefficient	K_m	Motor torque constant (lb-ft/A), $K_m = cK_e$
B	Bare-airframe control derivative matrix	K_p	Proportional ESC feedback gain
c	Torque SI unit conversion constant (0.7374 lb-ft/Nm)	L_a	Motor armature inductance (H or μ H)
C	Bare-airframe state output matrix	M	Motor rotational mass (slug)
D	Bare-airframe control output matrix	N_{spec}	Specification propulsion group engine speed (rpm or rad/s)
f_d	Drive system inertia factor	Q_A	Rotor aerodynamic torque (lb-ft)
H_{esc}	Motor speed controller transfer function	Q_S	Rotor shaft torque (lb-ft)
i_a	Motor armature current (A)	r	Drive system gear ratio
I_r	Main rotor rotational moment of inertia (slug ft ²)	R_a	Motor armature resistance (Ω)
J	Drive system rotational moment of inertia (slug ft ²)	s	Laplace domain variable (rad/s)
		t	Time (s)

Presented at the Vertical Flight Society's 76th Annual Forum & Technology Display, Virginia Beach, Virginia, USA, Oct. 6-8, 2020. This is a work of the U.S. Government and is not subject to copyright protection in the U.S.

t_r	Rise time (s)
V	Voltage (V)
V_a	Motor armature voltage input (V)
ΔI_{max}	Maximum current limit margin (A)
$\Delta \Omega_{max}$	Rotor speed change for ΔI_{max} (rad/s)
η	Motor efficiency factor
λ	Inductance proportionality constant
ϕ_I	Nominal motor voltage-to-current design ratio
ω	Motor speed (rad/s)
ζ	Damping ratio
Ω	Main rotor speed (rad/s)
τ	Motor shaft torque (lb-ft)

INTRODUCTION

Many current Urban Air Mobility (UAM) concepts include multirotor configurations. This is especially true for proposed all-electric, variable rotor speed-controlled vehicles in order to generate sufficient lift. While multirotor configurations are common for smaller aircraft, the handling qualities performance of configurations scaled for UAM application is still under investigation. Currently, there is no consensus on the number of rotors ideally suited for an application. Thus, a study of the optimal number of rotors and the impact on the design of the vehicle is required. When determining the correct number of rotors and type of control for a multirotor vehicle other factors such as power, mass, response, and stability must be considered in addition to lift generated.

The objective of this paper is to compare and contrast NASA Revolutionary Vertical Lift Technology (RVLT) Project's six-passenger quadcopter, hexacopter, and octocopter concept configurations in order to better inform design decisions on which multicopter and control type is appropriate for a range of applications. The study presented will focus primarily on increasing the handling qualities performance of the vehicle as this is, currently, one of the greatest challenges for enabling multirotor UAM configurations.

BACKGROUND

Malpica and Withrow-Maser (Ref. 1) investigated the method used to evaluate the control configurations for the RVLT UAM reference vehicles and compared the controllability of three quadcopters of various sizes (single passenger, four passenger, and six passenger) with variable blade pitch and variable rotor speed-controlled configurations. It was concluded that there were no drastic differences in the handling qualities performance of these vehicles based on size

because the control power laws scaled proportionally with the vehicle. However, it was determined that the variable rotor speed-controlled vehicle had significantly reduced stability margins than its variable blade pitch-controlled counterpart. In fact, with the cited assumptions, the rotor speed-controlled vehicle was not able to be controlled with Level 1 handling qualities (Ref. 2) with any usable bandwidth and reasonable limitations on power input. This paper will expand on adaptations to the vehicle design that would be necessary to increase the handling qualities performance of the variable rotor speed-controlled vehicle to Level 1 handling qualities standards as defined in Ref. 2. Additionally, the hexacopter and octocopter versions of the RVLT UAM concept reference vehicles will be examined to assess the impact of increasing the number of rotors on the vehicle design.

Handling qualities have been studied for small-scale multirotor unmanned aerial systems (UAS) with recommendations for adapting these scaled metrics to traditional ADS-33 Mission Task Elements (MTEs) in order to better evaluate performance of multirotor control designs. Additional efforts have been devoted to developing a quadrotor-specific Control Equivalent Turbulence Input (CETI) turbulence model (Ref. 3 and 4). Additionally, in collaboration with authors, Schuet, Kaneshige, and Lombaerts used a quasi-Linear Parameter Varying model and a Model Predictive Controller to look at the trade of handling qualities and motor requirements for the six passenger RVLT quadcopter reference vehicle. These efforts were done in preparation of a vertical motion simulator (VMS) test at NASA Ames to investigate performance trades of the variable speed and variable pitch quadcopters and the applicability of current handling qualities standards for passenger-sized multi-rotor vehicles (Ref. 5 and 6).

TECHNICAL APPROACH

The design process of the RVLT UAM reference vehicles can be found in Ref. 7. The six-passenger quadcopter was extended to a hexacopter and octocopter design for this study using NDARC. The vehicles were sized for the same set of missions and passengers, but other parameters such as rotor number, weight, power required, etc. vary. These vehicles were compared based on these characteristics and their ability to meet key performance requirements using the tools FlightCODE and CONDUIT. Ref. 1 showed that the collective-controlled variants of the concept quadcopter were reasonably stable, thus the first new objective is to determine what adaptations would be required to stabilize the variable rotor speed-controlled variant of the quadcopter. The second objective will be to compare this variable rotor speed-controlled variant with the hexacopter and octocopter to determine how the addition of rotor sets affected the handling qualities performance of the vehicle.

The control law configuration and optimization are automated in the FlightCODE process using CONDUIT (Ref. 2). FlightCODE utilizes the aircraft and performance files from NDARC to generate linearized stability and control derivative

matrices of the state-space system of equations that define the vehicle dynamics. Then, assuming a model-following control system architecture as in Figure 1 each axis of the vehicle is optimized separately for both feed forward and feedback in CONDUIT (for this application only the feedback will be discussed). The software attempts to stabilize the open-loop dynamics (if unstable) with robust command tracking performance and the ability to reject disturbance. CONDUIT tunes the control gains to handling qualities metrics with assigned priorities and then looks at the overall “cost” to determine an optimal system (Ref 2). For this study, the focus will be on the results of optimizing the electronic speed controller (ESC) as this allows rise time, stability, and damping capabilities to be compared between the three vehicle configurations. Supporting data will be obtained from the appropriate NDARC case file as required.

Control Implications

Using rotor speed as the primary control mechanism for the aircraft results in a more highly interconnected flight control and propulsion system than is usual in swashplate-controlled rotorcraft. A high-level diagram of the integrated vehicle electric propulsion and flight control systems is shown in Figure 1. Integrated propulsion and flight control systems such as these place the propulsion system directly in the open loop control path. Accounting for the dynamic response of the propulsion system is crucial to the control system design, because time lags or latency introduced by the motor dynamics in the open loop will have a determinant effect on the stability and performance of the control system when the feedback loop is closed, at the crossover frequencies required for maneuvering. Conversely, the requirements for maneuvering with good handling qualities will put additional demands on the motors in terms of the power margins required.

The stabilization of various quadcopter concepts, using rotor speed for control was explored in Ref. 1 with limited success. It was found that a large gap separates the collective-controlled and variable rotor speed-controlled quadcopter in terms of handling qualities performance. The control problem of the quadcopter was revisited here, focusing on the 6-passenger variant because this vehicle is seen as a more viable capacity for the UAM market.

THEORY

Motor Dynamics

The propulsion systems for the multirotor aircraft in the study are configured with one motor group per rotor, along the lines of the architectures described in Ref. 7. A gear box connects each rotor to its dedicated motor. This allows for an optimal weight solution trading off motor and transmission weights. Figure 2 shows the details of the motor model and the speed controller architecture.

As in Ref. 1, a simple first-order surrogate representation of the significantly more sophisticated dynamics of the permanent magnet synchronous motors expected of this type of electric propulsion system was adopted to adequately account for the response time constants. These are critical to the accurate estimation of the stability of the feedback system. This model captures the gross effects that govern the motor response dynamics.

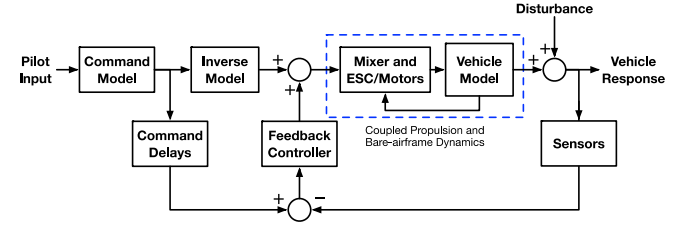


Figure 1. Model-following control system architecture with integrated vehicle propulsion.

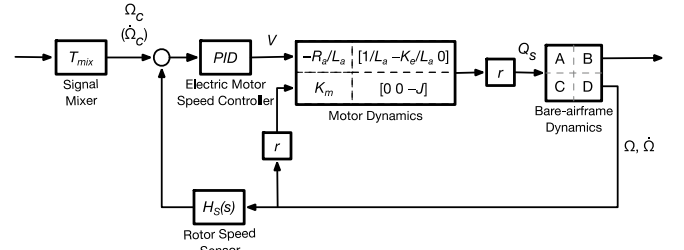


Figure 2. Block diagram of the electric motor and speed controller architecture.

In this basic model, the motor armature was assumed to have a coil with inductance, L_a , and resistance, R_a . Applying Kirchhoff’s Voltage Law to the circuit loop encompassing the windings of the motor armature yields

$$L_a \frac{di_a}{dt} = -R_a i_a - K_e \omega + V_a \quad (1)$$

where i_a is the current that circulates through the windings, $K_e \omega$ is the back-electromotive force (back-EMF) caused by the motor turning at its rotational speed, ω , and V_a is the voltage applied at the armature.

Coupled Rotor-Motor Dynamics. The motor torque delivered to the rotor shaft, after the gear box, is

$$Q_s = r \left(K_m i_a - J \frac{d\omega}{dt} - B\omega \right) \quad (2)$$

where r is the gear box ratio, $K_m i_a$ is the electrical motor torque output, which is proportional to the armature current i_a , J is the moment of inertia of the high-speed drive components (motor and coupled transmission components),

and B is a coefficient representing the mechanical friction or viscous losses in the drive system (but is currently assumed to be negligible for this study). Finally, note that motor constant K_m is related to the back-EMF constant through the relationship, $K_m = cK_e$, where the proportionality constant, c is the conversion factor between SI units (e.g., 0.7374 lb-ft/Nm). The motor speed ω is kinematically related to the rotor speed, so

$$\omega = r\Omega \quad (3)$$

The vehicle bare-airframe dynamics are represented by a linearized stability and control derivative model in state-space form and calculated using FlightCODE, formerly known as SIMPLI-FLYD (Ref. 2). Isolating the equations of motion that govern the rotor dynamics yields

$$I_r \frac{d\Omega}{dt} = \frac{\partial Q_A}{\partial \Omega} \Omega + \sum_{\rho_i \neq \Omega} \frac{\partial Q_A}{\partial \rho_i} \rho_i + Q_s \quad (4)$$

where I_r is the rotor inertia, Q_A is the rotor aerodynamic torque, and ρ_i are all other state and control variables that define the state-space system for the whole vehicle. Setting $\rho_i = 0$ for all i , and substituting shaft torque from Eq. (2), with $B = 0$, yields the coupled motor-rotor mechanical equation of motion

$$(I_r + Jr^2) \frac{d\Omega}{dt} = K_m r i_a + \frac{\partial Q_A}{\partial \Omega} \Omega \quad (5)$$

where Jr^2 is the contribution to the total moment of inertia of the motor and other high-speed drive components, such that the total angular momentum is $(I_r + Jr^2)\Omega$. Together, Eqs. 1 and 5 govern the dynamic response of the coupled motor-rotor system represented in Figure 2. The role of the PID motor speed controller is to specify the voltage input to the motor (Eq. 1) to ensure adequate tracking of the reference rotor speed commands.

Motor Parameter Characterization. The method for characterizing the motor dynamic response was introduced in Ref. 1. An equivalent approach was applied in Ref. 5. The philosophy behind the procedure described in Ref. 5 was to characterize motor dynamic and electrical parameters, which are otherwise absent from the sizing solution, using only the most basic information available from the vehicle sizing analysis. This approach is appropriate for this type of analysis with the consideration that detailed or specific motor data or models may not be available during the vehicle conceptual design stage.

Motor Back EMF. A slight change in the approach to motor parameter characterization was implemented for this study. To account for the influence of the nominal motor voltage-to-current ratio design point on the calculation of the motor back-EMF and related torque constant, motor voltage was assumed proportional to the current,

$$V = \varphi_I I \quad (6)$$

This approach allowed the design point to be biased to a higher or lower motor design voltage through the ratio, φ_I , an important consideration in the determination of the propulsion system designs. The mechanical power P delivered by the motor is ηVI , where η is the motor efficiency. It follows that

$$I = \sqrt{\frac{P}{\eta \varphi_I}} \quad (7)$$

The back-EMF constant (in SI units) is therefore given by

$$K_e = \frac{K_m}{c} = \frac{\tau}{cI} = \frac{\sqrt{\eta \varphi_I P}}{c\omega} \quad (8)$$

This approach allows the motor back-EMF constant to be calculated from an assumed (or known) motor efficiency at a given reference power available (e.g., P_{eng}) and speed (e.g., N_{spec}) operating condition. Alternatively, the constants could be estimated from the vehicle trim performance calculations for a given flight condition.

Motor Resistance. Considering the electrical power losses through the equivalent motor circuit resistance yields

$$R_a = \frac{1 - \eta}{\eta} \frac{(N_{spec})^2}{P_{eng}} K_e^2 \quad (9)$$

Inertia. Estimation of the motor rotating inertia depends on assumptions about the geometry (length to diameter aspect ratio and rotor to stator weight fraction) of the motor, where

$$J = \frac{1}{2} M \left(\frac{D_e}{2} \right)^2 f_d \quad (10)$$

is the moment of inertia of a cylinder of mass, M , and external diameter, D_e . Inertia factor, f_d , accounts in a simple way for high speed drive system components coupled to the motor and technology factors that may affect inertia.

A less conservative value of f_d was assumed for this study, with respect to that of Ref. 1, but in absence of actual data, this remains a design parameter choice.

Inductance. Motor inductance calculations from Ref. 1 were based on the empirical relationship

$$L_a = \lambda(\tau)K_e^2 \quad (11)$$

where

$$\lambda(\tau) = 244.22 - 0.7287\tau \quad (12)$$

is a function of the continuous torque rating $\tau = \tau_{MCP}$.

ESC OPTIMIZATION METHOD

The first goal of this study was to explore the control system design space to better understand the various trades in terms of the expected vehicle handling qualities and the motor power margins required. The model-following control system architecture in Figure 1 has been adopted for convenience of analysis at the conceptual design level because of the ability it provides for separating the feedback stability and performance properties from the vehicle response command shaping. A key aspect was understanding the achievable rotor speed response bandwidth (e.g., in terms of the rotor step response rise time) for various motor design parameters. However, the presence of the inner motor speed control loop (Figure 2) must be accounted for first.

Following conventional control system design practices, where various nested loops exist, the most inner loop is tuned first. Only Proportional Integral (PI) control was attempted at this time, so the Differential (D) feedback gain from the PID controller of Figure 2 was set to zero. The optimization objective of the motor speed controller gains was to minimize the closed-loop rotor speed step response rise time, subject to stability margin, closed-loop response damping ratio and steady state error, and motor current usage, or root-mean-square (RMS), constraints, according to Table 1. Notional definitions for the “good” and “bad” values in Table 1 were adopted in Ref. 8 and revisited in Ref. 1.

Table 1. Speed Controller Optimization Constraint Limits.

Parameters	Units	“Good”	“Bad”
Gain Margin	dB	7	6
Phase Margin	deg	60	45
Damping Ratio	-	0.9	0.8
Low-Frequency Magnitude ^a	dB	0.5	3.0
Motor Current – RMS ^b	-	1.5	2.0

^a 0.01–0.5 rad/s range, ^b Normalized

This approach allowed the solver to determine the quickest rotor response, while ensuring maximum motor usage was bounded. It is important to understand the definition of the motor usage metric, which is not of a direct physical significance. Given the closed-loop motor speed controller transfer function

$$H_{esc}(s) = \frac{i_a}{\Omega_c}(s) \quad (13)$$

defining the armature current response to a rotor speed command, the motor usage metric (i.e. motor current RMS metric) is defined to be proportional to the square root of the integral in the frequency domain of the output (i.e., the armature current) power spectral density function, $S_{i_a i_a}(\omega)$, such that

$$A_{rms} \propto \sqrt{\int_{\omega_1}^{\omega_2} S_{i_a i_a}(\omega) d\omega} \cdot \frac{\Delta\Omega_{cmax}}{\Delta I_{max}} \quad (14)$$

The metric weighs the bandlimited standard deviation (or RMS) of a process by integrating over the frequency range of interest for control. The value of the metric is normalized by the ratio of the specified maximum motor speed controller input ($\Delta\Omega_{cmax}$) and output (ΔI_{max}) limits. This normalization allows for the correct assessment of the magnitude of the process RMS, relative to the physical limits of the system. The maximum allowable rotor speed command limit was chosen to be ± 47 rpm (or about ± 5 rad/s), which corresponded to a 12% margin with respect to the hover rotor speed at the design flight condition. This maximum allowable rotor speed command was fixed for all design points to enforce a consistent and conservative constraint based on unknown potential aerodynamic or structural limits of the aircraft. It is noted that if left uncontrolled or unlimited, the motor could, in the linear world, command huge and potentially unsafe rotor speed changes if the maximum current were allowed to be commanded. From Eq. 5 it can be seen that in steady state conditions

$$\Delta\Omega_{max} = -\frac{K_m r}{\frac{\partial Q_A}{\partial \Omega}} \Delta I_{max} \quad (15)$$

Based on the chosen motor designs and current limits, the maximum rotor speed change could range from 3 to 55 rad/s (28 to 525 rpm).

In the motor models of Ref. 9, a constant motor efficiency of 95% was assumed. Without redesigning the vehicle, the effect of motor efficiency was parametrically explored to understand its effect on the dynamic response of the rotor and the motor speed controller design. The other parameter that was explored was the nominal voltage-to-current ratio design of the motor, with values ranging from 1 to 2.

Figure 3 shows the optimal rotor speed response rise time, or the time required for the rotor to respond to a pilot input, as a function of the maximum current limit, for various motor design parameters. Increasing the current limit allowed the controller to demand larger and more rapid torques from the motor. However, the rotor speed response rise time was subsequently found to converge to a minimum of approximately 0.08 s. This behavior is attributed, as shown in Figure 4, to the solution reaching the minimum allowable phase margin constraint. For the lower current limits, the solution was constrained by the motor current usage (RMS) specification. Between 200 and 600 A all solutions transitioned from the motor current RMS constraint to the stability phase margin constraint. This transition was accompanied by increasing feedback gains. Further increases would not have been possible without destabilizing the feedback loop. Note the increase in rotor speed response bandwidth was possible due to the relaxation of the current limit, but, in fact, the demands on the motor have increased and need to be quantified. In the following section these designs will be evaluated in the context of the whole vehicle stabilization and handling qualities.

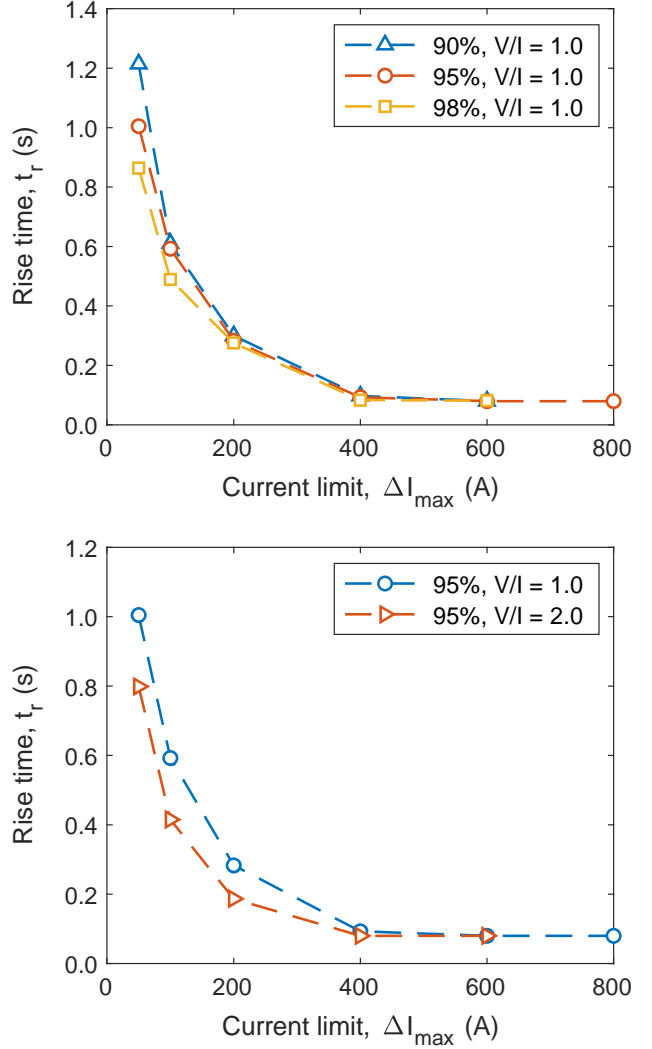
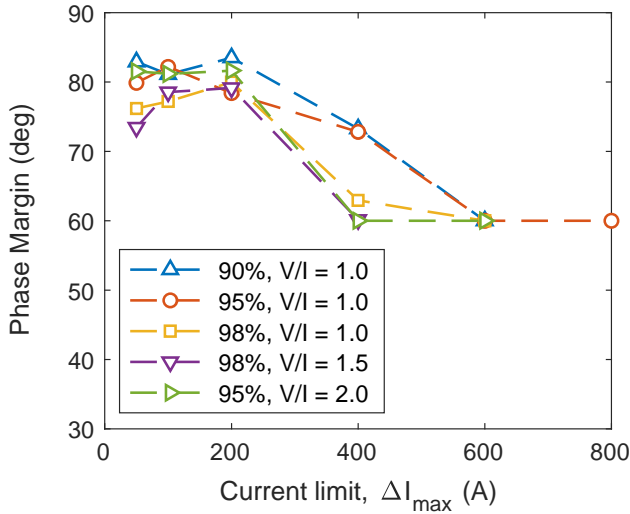
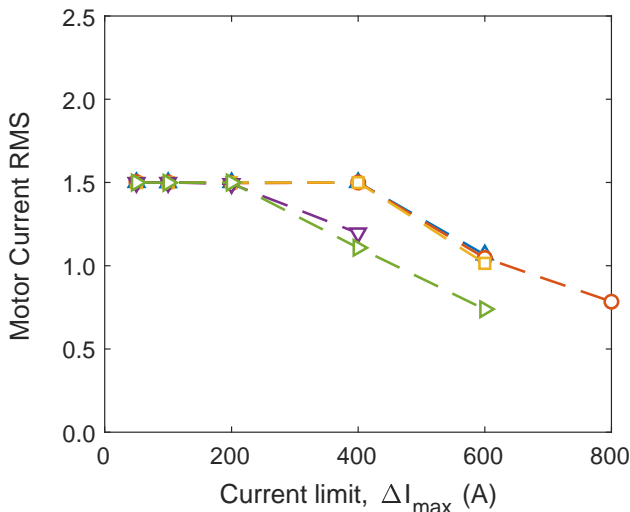


Figure 3. Rotor response rise time as a function of control optimization maximum current limit for various motor efficiencies and voltage to current design point ratios.



(a)



(b)

Figure 4. Motor speed controller optimization limiting constraints: (a) stability phase margin, and (b) motor usage

Qualification of Adequate Rise Time

The feedback controller of Figure 2 was configured as a PID compensator. The feedback gain optimization objective was set to minimize motor power usage, subject to stability and tracking performance constraints based on established control system design requirements for metrics such as stability margins, robustness, disturbance rejection bandwidth and peak, crossover frequency, eigen damping, among others. Stability margins, disturbance rejection bandwidth and mid-term response oscillations are some of the key metrics. Stability margin requirements for military aircraft are specified in the SAE Aerospace Standard AS94900A (Ref. 10) which calls for minimum phase and gain margins of 45 deg and 6 dB, respectively. The Aeronautical Design Standard, ADS-33E-PRF (Ref. 11) is the primary reference

specification document for handling qualities of military rotorcraft and establishes a minimum mid-term control response damping ratio requirement of at least 0.35 for attitude feedback systems. More recently, developments in the testing and validation of disturbance bandwidth (DRB) and peak (DRP) magnitude metrics in Ref. 12 have been proposed to be included into the next revision of ADS-33 (Ref. 13). For roll attitude feedback control systems, the disturbance rejection required is to be 0.9 rad/s at least. While aircraft certification under the various civilian aviation authorities does not require compliance with these standards, these are based on sound and proven engineering practices and provide objective numerical criteria for the control engineer to design to.

Feedback controller solutions were obtained for a variety of motor speed controller designs from Figure 3. The model of the motor with 95% efficiency and a nominal voltage-to-current ratio of 2.0 will be further discussed. This motor tended to offer the lowest rise times for current limits under 400 A. Two design approaches were taken: 1) the maximum current limit for the roll feedback problem definition was matched to the motor speed controller limit, and 2), disturbance rejection bandwidth constraints were varied for a constant maximum current limit of 50 A (with motor speed controller gains obtained for the limit of 100 A from Figure 3). The motor speed controller used for this second approach provided a rotor speed response rise time of about 0.42 s. This is in comparison with the rotor speed response rise time of about 0.8 s afforded by the motor speed controller that was optimized to a maximum current limit of 50 A.

Optimal motor usage, in terms of the scaled motor current RMS metric, for the various roll feedback design points, is shown in Figure 5. Figure 5 shows the matched current limit for the roll and motor speed controller from the first approach versus actuator usage as current limit is increased in blue. In red, Figure 5 shows the second approach where the current limit is held constant and disturbance rejection bandwidth is varied. The scaling effect of ΔI_{max} , when matching the maximum current limits to the motor speed controller design, is shown to cause the motor usage metric to decrease for the larger values of the current limits, so this comparison is not extremely useful. More informative are the stability margin, disturbance rejection and closed-loop eigen damping results of Figures 6–8. Figure 6 shows that increasing the maximum current limit caused both gain and phase stability margins to increase by 6 dB and 31 deg, approximately. The associated disturbance rejection (Figure 7) and eigen damping (Figure 8) characteristics were also improved by the controller solutions that were enabled by the larger maximum current limits. The roll disturbance rejection bandwidth rapidly increased from 0.6 rad/s to 0.9 rad/s (the multi-objective optimization constraint limit) for a maximum current limit of 100 A. Disturbance rejection peak decreased further, to about 1.7 dB, with increasing maximum current limits, after initially jumping to 3.3 dB for a limit of 100 A. The damping ratio for

eigenvalues between 0.5 and 4 rad/s, shown in Figure 8, followed similar trends with it increasing from 0.33 at 50 A to 1.0 at 200 A.

Crucially, the controllers designed to a constant limit of 50 A were generally able to achieve stable control designs with comparable performance, but with lower motor usage costs. The trade-offs between the roll disturbance rejection bandwidth and other key specifications for these control solutions are better illustrated in Figure 9. Note that motor usage in Figure 9 nearly doubles in order to achieve the required 0.9 rad/s DRB relative to the 0.56 rad/s design. To make physical sense of these motor current usage RMS metrics, it is necessary to correlate with motor power or torque margins. This will be the focus of the remainder of the paper, but from these results and prior results in Ref. 1, where a rotor speed step response rise time of about one second did not allow for vehicle stabilization with minimum 6 dB and 45 deg stability margins and 0.9 rad/s disturbance rejection bandwidth for the concept six-passenger quadcopter, it can safely be argued that rise times between 0.4 and 0.8 s are likely sufficient to stabilize the vehicle with good feedback control performance characteristics. Given a rise time of 0.42 s, phase margin (and, consequently, roll damping) could be traded for increased disturbance rejection bandwidth (Figures 6–8 and Figure 9). A rise time of 0.8 s barely afforded the roll feedback compensator with the minimum required phase margin (Figure 6) and is not likely to satisfy minimum requirements for all specifications for DRB (Figure 7 and eigen damping (Figure 8)). These rise times will be extrapolated to the six- and eight-rotor designs where the study will be focused on the motor speed controller optimization and correlation of motor current usage RMS metric limits to power margins.

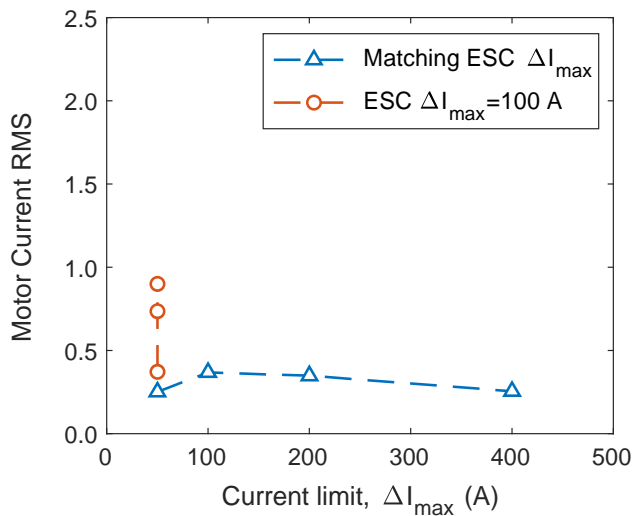


Figure 5. Motor usage for various roll axis feedback designs.

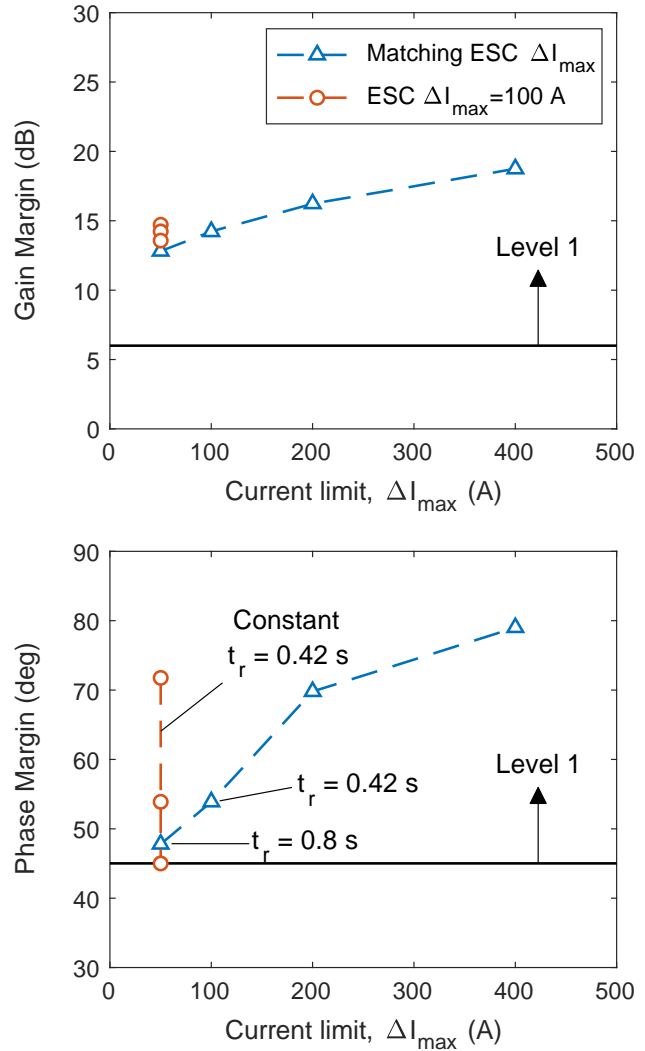


Figure 6. Stability margins for various roll axis feedback designs.

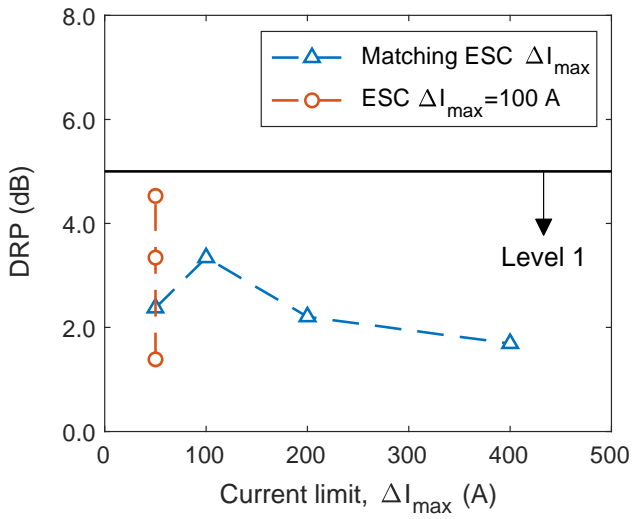
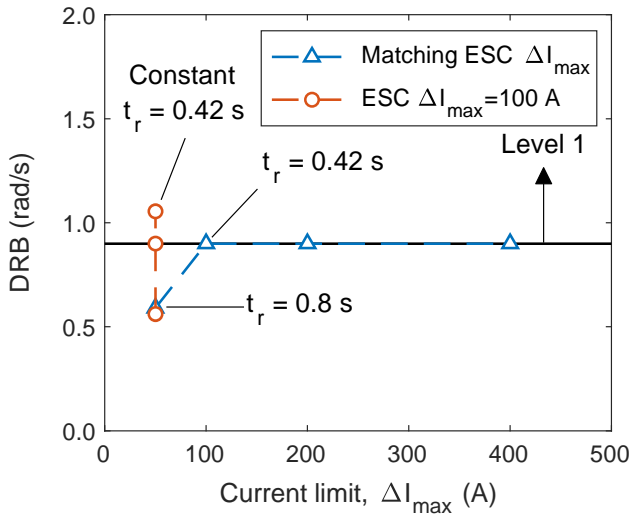


Figure 7. Disturbance rejection (bandwidth and peak) for various roll axis feedback designs.

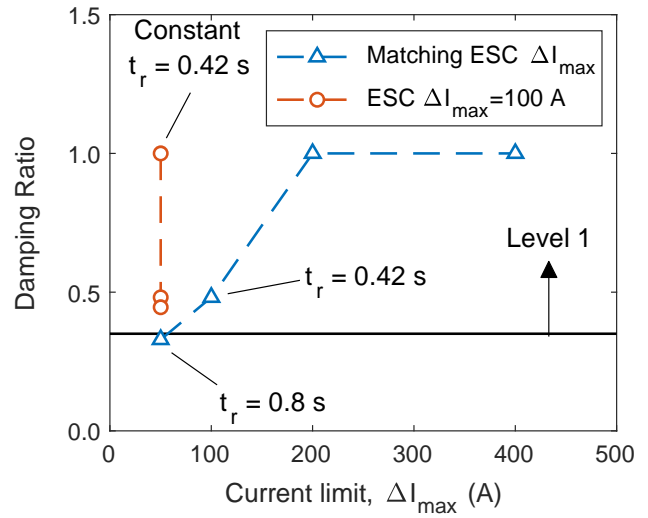


Figure 8. Roll eigen damping for various roll axis feedback designs.

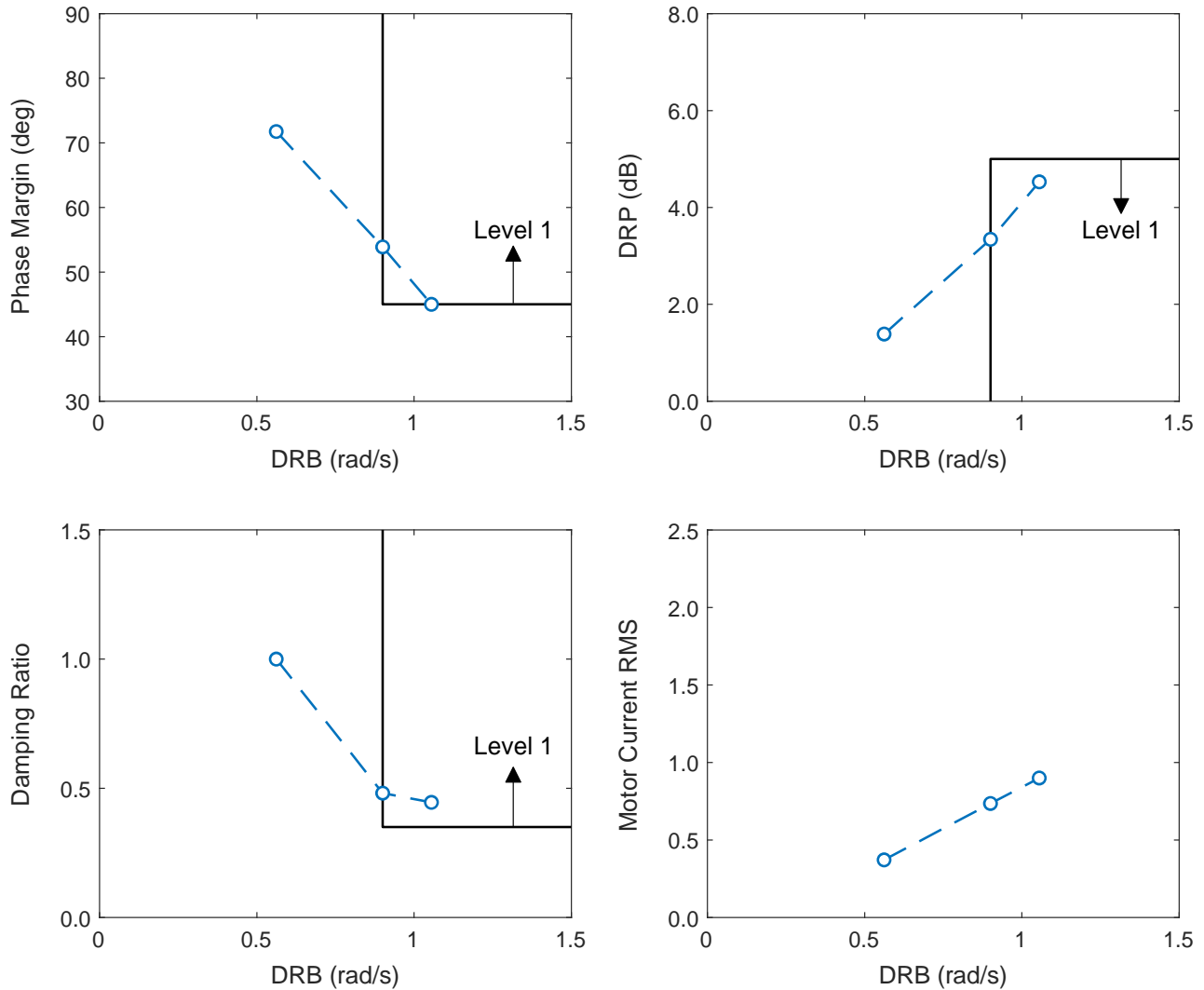


Figure 9. Disturbance rejection bandwidth trade-off for a motor speed controller with $t_r = 0.42$ s.

EXTENSION TO HEXACOPTER AND OCTOCOPTER MODELS

Using the quadcopter as a base, sets of rotors were added to create NDARC models of a hexacopter and an octocopter consistent with the methodology described in Ref. 14. While number of rotors and associated components (batteries, hubs, etc.) were added to the original model, all three vehicle configurations were sized to the same mission scope for six passengers and used variable rotor speed for control. The second objective of this study was to compare the variable rotor speed-controlled variant of the quadcopter with the hexacopter and octocopter to determine how the addition of rotor sets affected the ability of the vehicle to reach Level 1 handling qualities. The authors theorized that adding more rotors would improve handling qualities performance as additional rotors mean that smaller rotor radii are required for

the same overall disk area. Smaller rotors lead to smaller rotor inertias and, theoretically, less power per motor for adequate rise times. As mentioned above, the torque and power limits available in the model of Ref. 1 were insufficient for designing a motor speed control system with adequate rise time. Analysis of the quadrotor, above, settled on an increased voltage/current ratio of 2.0 because it allowed slightly better rise times of the motor speed control loop for the same maximum current limit. Thus, to match the quadrotor design, motor efficiency was fixed to 95% and a voltage/current ratio of 2.0 for analysis of all hexacopter and octocopter designs.

The same method described earlier in this section for the quadcopter was used to optimize the ESC of the hexacopter and octocopter using FlightCODE and CONDUIT. The ESC optimization of all three vehicles were able to converge to “good” parameters as defined in Table 1 with an adequate rise

time (0.4-0.8 s) for input limits found in Table 2. (Note, that this does not necessarily mean that all three vehicles will meet Level 1 handling qualities.) Like the quadcopter, a tradeoff was evident between stability and damping ratio. The margin for the crossover frequency into the “good” range increased as current limits were increased. Rise time could be decreased by increasing the motor current RMS usage with reduced stability. For both the hexacopter and octocopter, these low rise times could be reached with significantly less power per motor than their quadcopter counterpart. However, even with significant power available, the rise time was never lower than 0.08 s, the same “limit” as the quadcopter. Figure 10 shows the rate at which each vehicle converged to the minimum rise time. It should also be noted that the octocopter took more iterations to reach the minimum rise time than the other two vehicles, even though it took very few iterations to reach “good” parameters as defined in Table 1. Additionally, the solver sometimes required a manual input to minimize rise time, suggesting that there were likely multiple local solutions (though confirmation of this theory was left for future work). It was determined that a satisfactory solution had been reached when one of the parameters listed in Table 1 was at the boundary between the “good” and “bad” parameters.

The difference between the three vehicle configurations was most noticeable in the power required to reach the range of desirable rise times and the corresponding torque margins. It should be noted that all of the runs that fall into the “ideal” rise time range are in the range of 0 to ~100 A maximum current limit. While the vehicle is not unstable at lower rise times and higher currents, more power is required than is necessary to meet the requirements as defined in Table 1. Figure 10 shows that most of the rise times below 0.4 s require more than a current limit of 100 A.

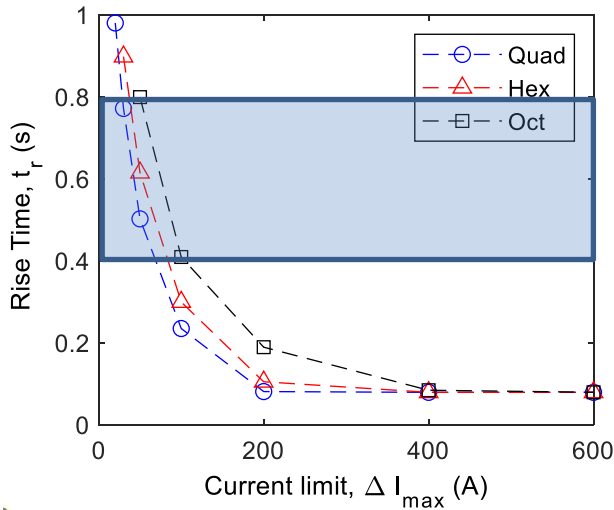


Figure 10. Current limit versus rise time with the shaded region showing the desirable rise time region between 0.4 and 0.8 s (shaded region) for a single motor- $\eta=95\%$, $V/I=2.0$.

Power

Interpolation was used to determine the associated maximum current limit for the rise times of 0.4 and 0.8 s, the range of interest for desirable handling qualities. Associated mechanical power trends were determined using Eq. 16, derived from Eq. 8. MRP

$$P_{Mech} = \tau\omega = K_m(I_o + \Delta I_{max})(\Omega_o + \Delta\Omega)r \quad (16)$$

The mechanical power trends (Figure 11) determine the required power for a single (front) motor to reach the desired rise time range. Current limit and mechanical power associated with the range of 0.4 to 0.8 s rise time can be found in Table 2. It is important to note that much of the region in Figure 11 reflects power values that are higher than the maximum rated power of the vehicle (MRP) (Table 2). The NDARC model already includes predicted technology factors in the vehicle design, therefore, a vehicle redesign and enhanced power system would be required to utilize regions of the graph where the power values are greater than the MRP.

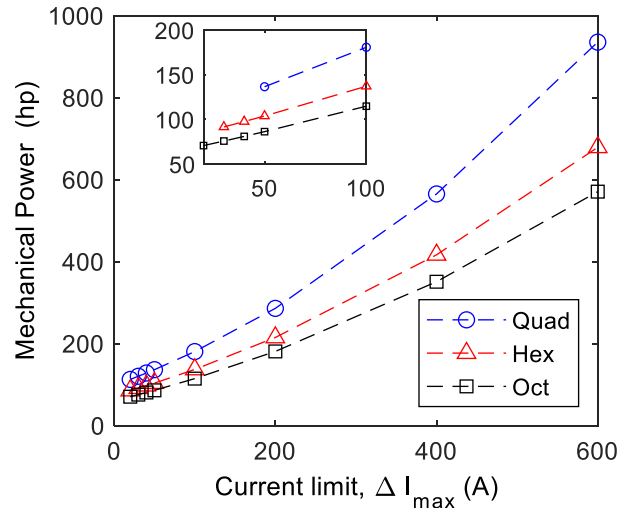


Figure 11. Mechanical Power for Motor 1 required versus maximum current for three six passenger vehicle configurations.

Table 2. Current Limit and Power Bounds Associated with Desirable Rise Time per (Front) Motor.

	Units	Quad	Hex	Oct
Current Limit (rise time 0.8 s)	A	28.7	37.1	50.0
Power Required (rise time 0.8 s)	hp	119.5	95.9	86.3
Current Limit (rise time 0.4 s)	A	69.9	84.3	104.6
Power Required (rise time 0.4 s)	hp	153.3	126.6	117.3
MRP	hp	130.5	101.5	94.7

For all three vehicles, low current limits were associated with high rise times and, inferred, worse handling qualities. The hexacopter required less power per motor to meet the same rise times as the quadcopter, and the octocopter required the least amount of power per motor of the three configurations to reach the desired rise times.

Next, the power required for control was compared to the power required for hover and the MRP in Table 3 at a range of ΔI_{max} inputs.

Table 3. Power Required and Rise Time ($\Delta I_{max} = 50$ A).

Parameters	Units	Quad	Hex	Oct
MRP	hp	130.5	101.5	94.7
Vehicle control (Rotor)	hp	136.6	103.8	86.3
Vehicle control (Motor)	hp	146.1	110.6	92.8
Hover (Rotor)	hp	96.9	73.3	60.1
Control Power Ratio (Rotor)	-	1.410	1.416	1.435
Rise time	s	0.8	0.616	0.503

All values in Table 3 are for a ΔI_{max} of 50 A. In Table 3, rotor shaft power required for vehicle control is calculated from Eq. 16. Transmission and accessory losses are added to determine motor shaft required for vehicle control. The vehicle can only operate at MRP for short durations. Therefore, it is used here as a limit for the current design of the vehicle. Rotor shaft power required to hover is calculated by setting the perturbation quantities in Eq. 16 to zero. Here, the control power ratio is defined as the ratio of rotor shaft power to control the vehicle to motor shaft power required to hover characterizes the power requirements over the value required to trim in hover to control the vehicle. This additional power could potentially be achieved in a future iteration of the vehicle design, but power systems and batteries with increased technology factors would still be required for this

vehicle to become a reality. The power required for control power ratio shows that there is little difference between the three vehicles configurations regarding the margin of power required to for controllability. However, it is significant that for similar power margins, the hexacopter and octocopter have significantly lower rise times that the quadcopter, with the octocopter being the lowest of the three configurations at about 0.5 s.

It should also be noted that for the quadcopter, 50 A is the boundary of the usable rise time (0.8 s). Therefore, while meeting this performance specification is a key performance metric, it is likely that additional power may be required for all essential maneuvers to fall in Level 1 handling qualities range. Thus, the power was also investigated at higher ΔI_{max} input values (Tables 4 and 5).

Table 4. Power Required and Rise Time ($\Delta I_{max} = 100$ A).

Parameters	Units	Quad	Hex	Oct
MRP	hp	130.5	101.5	94.7
Vehicle control (Motor)	hp	190.3	144.0	121.3
Hover (Rotor)	hp	96.9	73.3	60.1
Control Power Ratio (Rotor)	-	1.866	1.870	1.910
Rise time	s	0.410	0.300	0.236

Table 5. Power Required and Rise Time ($\Delta I_{max} = 200$ A).

Parameters	Units	Quad	Hex	Oct
MRP	hp	130.5	101.5	94.7
Vehicle control (Motor)	hp	295.7	222.0	187.6
Hover (Rotor)	hp	96.9	73.3	60.1
Control Power Ratio (Rotor)	-	2.954	2.935	3.013
Rise time	s	0.190	0.106	0.082

Except for the octocopter with a ΔI_{max} of 100 A, the values in Table 4 and 5 are outside of the rise time window of 0.4-0.8 s. However, they represent a benchmark and show trends for the values that are likely more representative of what would be needed for more extreme maneuvers. Just like the ΔI_{max} of 50 A case, the higher input current limits have similar margins across the configurations, but the octocopter has the least rise time for that margin.

Torque

Rotor torque trends were determined using Eq. 17 in the same manner as the power trends for a single (front) motor. Figure 12 shows these trends. Rotor and motor torque for $\Delta I_{max} = 50$ A can be found in Table 6.

$$Q_s = K_m(I_o + \Delta I_{max})r \quad (17)$$

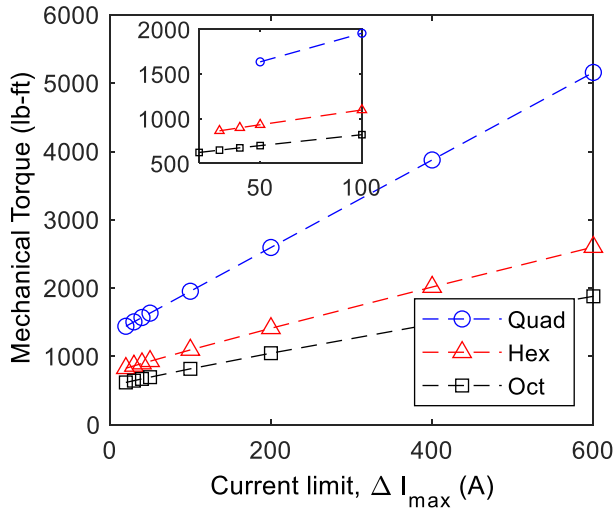


Figure 12. Rotor torque for Motor 1 generated versus maximum current for three six passenger vehicle configurations.

Table 6. Torque Required and Rise Time ($\Delta I_{max} = 50$ A).

Parameters	Units	Quad	Hex	Oct
Vehicle Control (Rotor)	lb-ft	1634.6	971.7	742.0
Vehicle Control (Motor)	lb-ft	94.0	65.2	55.3
Drive System Limit	lb-ft	1947.5	1155.4	894.4
Hover (Rotor)	lb-ft	1314.3	758.5	567.1
Hover (Motor)	lb-ft	76.9	51.9	43.2
Control Torque Ratio (Rotor)	-	1.244	1.281	1.308
Control Torque Ratio (Motor)	-	1.222	1.258	1.279
Rise Time	s	0.800	0.616	0.503

Torque required and torque limits are shown in addition to power (in the previous section) as it is possible that a mechanical torque limit will be exceeded before a power limit. For this work, only the 50 A current margin input will be discussed. Just like the power trends, the 50 A current margin limit case is on the edge of the usable rise time range (0.8 s) for the quadcopter. The rotor shaft torque required for control was calculated using Eq. 17. Motor shaft torque, τ , required for control accounts for the transmission and accessory losses. The drive system torque limit is sized in NDARC for the design and influences drive system weight. Rotor torque required for hover is calculated by setting the current perturbation to 0 in Eq. 17. Motor torque required for hover accounts for the transmission and accessory losses between the motor and rotor. Rotor control torque ratio is

defined as the torque required for the rotor to control the vehicle to the rotor torque required for hover. Motor control torque ratio accounts for the transmission and accessory losses. Just like the power study, the control torque ratios are similar, but the octocopter has a lowest rise time of the three vehicles.

OTHER CONSIDERATIONS

Like any design process, increased handling qualities performance must be traded with other design considerations such as weight, aerodynamic interference, acoustics, and mission. For reference, common parameters of the vehicle configurations can be found in Table 7. Trim metrics correspond to the rotor values required to hover and were derived from Eqs. 8, 16, and 17 where perturbations were set to 0. All other values are associated with the NDARC model for each vehicle configuration.

Table 7. Consistent Design Parameters.

Parameter	Unit	Value
Payload Weight	lb	1200
Number of Blades	-	3
Disk Loading	lb/ft ²	3.0
Solidity, thrust weighted	-	0.055
Hover Tip Speed	ft/s	550
Flapping Frequency	per rev	1.03
Range	nm	75

Key differences in the designs can be found in Table 8.

Table 8. Key Design Differences between the Quad-, Hexa-, and Octo-copter Configurations.

	Units	Quad	Hex	Oct
Rotor Radius	ft	12.3	10.5	9.5
Design Gross Weight	lb	5716.4	6210.7	6846.8
Avg. Design Power Available per rotor	hp	147.8	114.2	98.7
Total Design Power	hp	591.3	685.3	789.8
Reference Rotational Speed	rad/s	44.7	52.5	57.7
Rotor Inertia	slugs ft ²	202.6	100.7	66.7
Motor Inertia (slugs ft ²)	slugs ft ²	0.047	0.033	0.027
Motor constant, Km (V/I=2, η=95%)	lb-ft/A	0.3415	0.2672	0.2410
r, Gear ratio	-	18.75	15.96	14.52
Trim Current	A	205.2	177.8	162.1
Trim Power (hover)	hp	96.9	73.3	60.1
Trim Torque (hover)	lb-ft	1314.3	758.5	567.1

Increasing the number of rotors from a quadcopter configuration to a hexacopter or octocopter configuration puts less torque and lower power requirements on the individual rotors. Also, in an emergency situation where a motor or rotor becomes inoperable, the vehicle may be easier to handle as it lands with six or eight rotors, instead of four. However, as seen in Table 8, design gross weight and total power required become larger for each set of rotors that is added. Additionally, wake interference and acoustics become more complex. The ideal number of rotors for each vehicle will need to be chosen based on priorities of the mission, environment in which the vehicle will fly, and risk factors. However, the importance of handling qualities performance should not be underestimated for UAM vehicles. Sufficient handling qualities performance is key to safety as these vehicles will be required to operate in close proximity to buildings and large populations and may experience atypical wind gusts from the urban environment.

FUTURE WORK

ESC optimization has been completed for the hexacopter and octocopter. Future work includes expanding this analysis to the heave, roll, pitch, and yaw axes. Along with this study, additional validation of the disturbance rejection boundaries

is required. This will be addressed as part of an upcoming task in the Vertical Motion Simulator (VMS) at NASA Ames for the variable blade pitch- and variable rotor speed-controlled versions of the quadcopter. Placement of rotors should be looked at in addition to the number of rotors. Placement of the rotors could significantly affect the forces and moments experienced by the vehicle at a given time. Lastly, while the addition of rotor sets has desirable effects on handling qualities performance in the configurations studied in terms of the rotor speed response rise time, it is uncertain if these benefits would extend to configurations with greater than eight rotors, and at what point the additional stresses, complexity, and aerodynamic interference would negate any benefits from adding rotor sets.

CONCLUSIONS

Many contemporary UAM vehicle designs are dependent on variable blade pitch controls and multiple rotors. Increased battery efficiency and more efficient motors will be required to enable this reality. However, with high enough control power, these vehicles can be stabilized. The next challenge for engineers will be to determine the best manner to provide that control power. Shaft torques can also be a limiting factor for designing usable control systems for variable rotor speed-controlled vehicles as well as power limits. Hexacopter and octocopter vehicles have more mass and require more power overall than a quadcopter, but control power ratio and control torque ratio remain similar across the vehicle configurations. The octocopter can achieve a lower rise time for these ratios than the hexacopter or quadcopter in the cases studied.

Author contact: Shannah Withrow shannah.n.withrow@nasa.gov, Carlos Malpica carlos.a.malpica@nasa.gov, Keiko Nagami keiko.nagami@nasa.gov.

ACKNOWLEDGMENTS

The authors would like to thank Dr. Wayne Johnson and Chris Silva for creating the NASA UAM reference vehicles. Thank you also to Stefan Schuet for providing feedback.

REFERENCES

- [1] Malpica, C. and Withrow-Maser, S., "Handling Qualities Analysis of Blade Pitch and Rotor Speed Controlled eVTOL Quadrotor Concepts for Urban Air Mobility," Vertical Flight Society International Powered Lift Conference 2020 Proceedings, San Jose, CA, January 21–23, 2020.
- [2] Lawrence, B., Theodore, C.R., Johnson, W., T. and Berger, T., "A Handling Qualities Analysis Tool for Rotorcraft Conceptual Designs," *The Aeronautical Journal*, Vol. 122 No. 1252 960, June, 2018, pp. 960–987.
- [3] Cheug, K., Wagster, J., Tischler, M., Ivler, C., Berrios, M., Berger, T., Ca, R., Lehmann, Juhasz, O., Tobias, E., Goerzen,

- C., Barone, P. Sander, F., and Lopez, M., "An Overview of the U.S. Army Aviation Development Directorate Quadrotor Guidance, Navigation, and Control Project," American Helicopter Society 73rd Annual Forum Proceedings, Fort Worth, TX, May 2017.
- [4] Ivler, C., Goerzen, C., Wagster, J., Sanders, F., Cheung, K., and Tischler, M., "Control Design for Tracking of Scaled MTE Trajectories on an IRIS+ Quadcopter," American Helicopter Society 74th Annual Forum Proceedings, Phoenix, AZ, May 2018.
- [5] Schuet S., Malpica, C., Lombaerts, T., Kaneshige, J., Withrow-Maser, S., Hardy, G. and Aires, J., "A Modeling Approach for Handling Qualities and Controls Safety Analysis of Electric Air Taxi Vehicles," AIAA Aviation Forum Proceedings, Modeling and Simulation Technologies Conference, June 15–19, 2020.
- [6] Lombaerts, T., Kaneshige, J., and Feary, M., "Control Concepts for Simplified Vehicle Operations of a Quadrotor eVTOL Vehicle," AIAA Aviation Forum Proceedings, Virtual Event, June 15-19, 2020.
- [7] Johnson, W., Silva, C., and Solis, E., "Concept Vehicles for VTOL Air Taxi Operations," American Helicopter Society Technical Conference on Aeromechanics Design for Transformative Vertical Flight Proceedings, San Francisco, CA, January 16–19, 2018.
- [8] Walter, A., McKay, M., Niemiec, R., Gandhi, F. and Ivler, C., "Handling Qualities Based Assessment of Scalability for Variable-RPM Electric Multi-Rotor Aircraft," Vertical Flight Society 75th Annual Forum Proceedings, Philadelphia, Pennsylvania, May 13-16, 2019.
- [9] Silva, C., Johnson, W., Antcliff, K. R., and Patterson, M. D., "VTOL Urban Air Mobility Concept Vehicles for Technology Development," AIAA Aviation Forum Proceedings, Aviation Technology, Integration, and Operations Conference, Atlanta, GA, June 25–29, 2018.
- [10] Anon., "Vehicle Management Systems - Flight Control Function, Design, Installation and Test of Piloted Military Aircraft, General Specification For," SAE Aerospace Standard, AS94900A, August 2018.
- [11] Anon., "Handling Qualities Requirements for Military Rotorcraft," Aeronautical Design Standard-33 (ADS-33E-PRF), US Army Aviation and Missile Command, March 2000.
- [12] Berger, T., Ivler, C. M., Berrios, M.G., Tischler, M.B., and Miller, D. G., "Disturbance Rejection Handling Qualities Criteria for Rotorcraft," American Helicopter Society 72nd Annual Forum, West Palm Beach, FL, May 17–19, 2016.
- [13] Blanken, C. L., Tischler, M. B., Lusardi, J.A., Berger, T., Ivler, C. M., and Lehmann, R., "Proposed Revisions to Aeronautical Design Standard – 33E (ADS-33E-PRF) Toward ADS-33F-PRF," U.S. Army Combat Capabilities Development Command, Special Report FCDD-AMV-19-01, September 2019.
- [14] Johnson, W., "NDARC NASA Design and Analysis of Rotorcraft," NASA TP-2009-215402, 2009.